

The Ultraviolet Radiation Environment of a Tropical Megacity in Transition: Mexico City

2000-2019

Adriana Ipiña,^{*,†,‡} Gamaliel López-Padilla,[¶] Armando Retama,[§] Rubén D. Piacentini,[†] and Sasha Madronich^{||}

[†]*Instituto de Física Rosario (CONICET-UNR), Rosario, Argentina*

[‡]*Centro de Ciencias de la Atmósfera, Universidad Nacional Autónoma de México, Mexico City, Mexico*

[¶]*Facultad de Ciencias Físico Matemáticas, Universidad Autónoma de Nuevo León, San Nicolás de los Garza, México*

[§]*Independent researcher, Mexico City, Mexico*

^{||}*National Center for Atmospheric Research, Boulder, Colorado, USA*

E-mail: ipina@ifir-conicet.gov.ar

Abstract

Tropical regions experience naturally high levels of UV radiation, but urban pollution can reduce these levels substantially. We analyzed 20 years of measurements of the UV Index (UVI) at several ground-level locations in the Mexico City Metropolitan Area and compared these data with UVI values derived from satellite observations of ozone and clouds (but not local pollution). The ground-based measurements were systematically lower than the satellite-based estimates, by ca. 40% in 2000 and 20% in 2019. Calculations with a radiative transfer model and observed concentrations of

9 air pollutants explained well the difference between satellite- and ground-based UVI,
10 and showed specific contributions from aerosols in the boundary layer and the free tro-
11 posphere, O₃, NO₂, and SO₂, in decreasing order of importance. Such large changes
12 in UV radiation between 2000 and 2019 have important implications ranging from hu-
13 man health (skin cancer and cataract induction) to air pollution control (photochemical
14 smog formation).

15 Introduction

16 Ultraviolet (UV) radiation is an important component of the urban environment, affecting
17 human populations directly through UV exposure of skin and eyes^{1–3} and less directly (but
18 with great impact) by driving the formation of photochemical smog, including tropospheric
19 ozone and other oxidants, as well as secondary aerosols containing nitrates, sulfates, and
20 organics.^{4–6} These pollutants, along with others of primary origin commonly found in ur-
21 ban atmospheres (e.g., black carbon, sulfur dioxide), can in turn scatter and/or absorb UV
22 radiation, alter its vertical distribution, and so modify the photochemical rate of their own
23 formation. Such feedback complicates the calculation of both the UV radiation field (in-
24 cluding at the surface), and the evolution of photochemical smog in the urban boundary
25 layer.

26 The question of how air pollution alters the urban UV environment (and *vice versa*) is
27 not new, but studies have relied mostly on numerical models,^{7–9} with relatively few available
28 observations (e.g., McKenzie et al.¹⁰, Panicker et al.¹¹, Palancar et al.¹², reviewed by Bais
29 et al.¹³). Increases in UV have been estimated as a consequence of emission reductions
30 over the last decades, e.g. in China,^{14–16} and have led to less-than-expected reductions in
31 photochemical smog, in part due to stronger UV photochemistry.^{17–19} Emission reductions
32 have also occurred globally during the 2020 COVID-19 pandemic,^{20,21} but ground-level ozone
33 in some polluted areas has actually increased,^{22,23} due at least in part to the increased UV
34 radiation. Unfortunately, the observational data base of relevant UV radiation remains

35 rather sparse to evaluate such model-derived hypotheses.

36 The environment of Mexico City is of particular interest for several reasons: (1) Nearly
37 23 million people inhabit the Mexico City Metropolitan Area (MCMA), and the UV en-
38 vironment has direct implications for their health, both in terms of skin/eye UV exposure
39 and *via* photochemical smog formation. (2) As a tropical megacity, it is to some extent
40 representative of the situation of many others, with year-round intense midday UV irradia-
41 nce, a shallower atmosphere due to the city's high elevation of 2240 m above sea level,
42 and a transition toward newer and cleaner technologies, leading to gradual improvements
43 in air quality. (3) Air quality within MCMA has undergone extensive scrutiny, with a well-
44 established monitoring network operating since 1986,²⁴ numerous intensive field campaigns
45 to study the meteorology, emissions, and photochemistry of smog formation,^{25–27} and numer-
46 ical modeling incorporating the evolving knowledge.^{28–31} This extensive body of knowledge
47 provides the foundation for understanding our study.

48 Here, we analyze two decades of continuous measurements of the UV Index at multiple
49 locations within the MCMA, collected by the Secretariat of the Environment (Secretaría
50 del Medio Ambiente, SEDEMA)¹ of the Mexico City government as part of an intensive
51 monitoring network over the MCMA. The UV Index is defined as:

$$UVI = 40 \int_{250nm}^{400nm} E(\lambda, t) \cdot S_{er}(\lambda) d\lambda \quad (1)$$

52 where $E(\lambda, t)$ is the solar spectral irradiance in units of $\text{W} \cdot \text{m}^{-2} \cdot \text{nm}^{-1}$ and $S_{er}(\lambda)$ is
53 the erythemal sensitivity of human skin.^{32,33} Multiplication by 40 was chosen historically to
54 express the UVI in small integer numbers, but is otherwise scientifically arbitrary.

55 The UVI is recognized by the World Health and Meteorological Organizations (WHO
56 and WMO) as a standardized metric of UV radiation³² for global public information. An
57 advantage of using the UVI as (one) measure of UV radiation is that it is being increasingly
58 observed or calculated and disseminated, enabling more objective comparisons among seasons

¹<https://www.sedema.cdmx.gob.mx/>

59 and locations. The UVI observations from Mexico City, considered here, are an important
60 element of this global picture.

61 While the UVI at the surface cannot be translated directly into photolysis frequencies
62 for various photo-labile molecules, the spectral weighting of the UVI (ca. 300-320 nm) is
63 approximately similar to that for the photolysis of ozone to singlet oxygen atoms. Other UV
64 wavelengths are of course also important, e.g. for the photolysis of nitrogen dioxide, and
65 may be affected differently depending on the pollutant. With these considerations and a few
66 other caveats, UVI trends examined here can also be used to infer accompanying trends in
67 photolysis frequencies and influences on photochemical smog formation.

68 Methods

69 Ground-based measurements

70 The Mexico City Metropolitan Area is located at 19.4°N, 99.1°W, 2240 meters above sea
71 level (m asl), surrounded by mountain ridges exceeding 5000 m asl, with complex topog-
72 raphy and thermal inversions that inhibit winds and favor intense air pollution.³⁴⁻³⁶ Air
73 quality monitoring and surface meteorological measurements in the MCMA are conducted
74 continuously by the Automated Atmospheric Monitoring Network (RAMA, by its Spanish
75 acronym) of the Atmospheric Monitoring System (SIMAT, by its Spanish acronym) of the
76 Mexico City government. Since the year 2000, UV radiometers (model 501-A, Solar Light
77 Company Inc., Glenside, PA) detecting wavelengths between 280-400 nm have been mea-
78 suring erythemally-weighted solar radiation. The calibration of the UV sensors has been
79 carried out annually by comparing against a factory-calibrated reference sensor. The out-
80 put voltages from the network's sensors have been compared for at least one week against
81 the UV readings from the reference sensor to derive a calibration factor. New calibration
82 factors typically differ from the old ones by 2% or less. Reference sensors have been also
83 calibrated by the manufacturer and updated periodically (between 3 to 5 years) to reduce

84 systematic errors due to drifts in sensitivity. Long term calibration drift are minimized by
 85 these yearly re-calibrations. Although at the beginning only a few stations were in oper-
 86 ation and have been changing, currently 11 stations are recording erythemal irradiances,
 87 which are then multiplied by 40 (see Eq. 1) to give UV Indices. Table 1 describes the lo-
 88 cation of the stations where the UV Index has been measured. Figure 1 shows how the
 89 radiometers of the SIMAT have been distributed over MCMA, prioritizing sites with higher
 90 population density. Near real-time data for each station are available on the SIMAT official
 91 website <http://www.aire.cdmx.gob.mx/default.php>. Daily maximum values (UVI_{max})
 92 were extracted in each of the stations around solar noon from the time interval from 11:00
 93 h-15:00 h CST (Central Standard Time). This database with 7305 continuous days of mea-
 94 surements during the period 2000-2019 was analyzed.

Table 1: SIMAT stations and AERONET site*, environmental descriptors and geographical positions. Abbreviations names: Chalco (CHA), Cuautitlán (CUT), FES Acatlán (FAC), Hangares (HAN), Laboratorio de Análisis Ambiental (LAA), Merced (MER), Montecillo (MON), Milpa Alta (MPA), Pedregal (PED), San Agustín (SAG), Santa Fe (SFE), Tlalnepantla (TLA) and National Autonomous University of Mexico (UNAM*)

Station	Environment	Lat (°N)	Lon (°W)	El (m asl)
CHO	semi-urban	19.27	98.89	2253
CUT	ecological park	19.72	99.20	2263
FAC	urban	19.48	99.24	2299
HAN	urban	19.42	99.08	2235
LAA	urban	19.48	99.15	2255
MER	downtown	19.42	99.12	2245
MON	rural	19.46	98.90	2252
MPA	rural	19.18	98.99	2594
PED	residential	19.33	99.20	2326
SAG	urban	19.53	99.03	2241
SFE	residential	19.36	99.26	2599
TLA	urban	19.53	99.20	2311
UNAM*	University city	19.33	99.18	2294

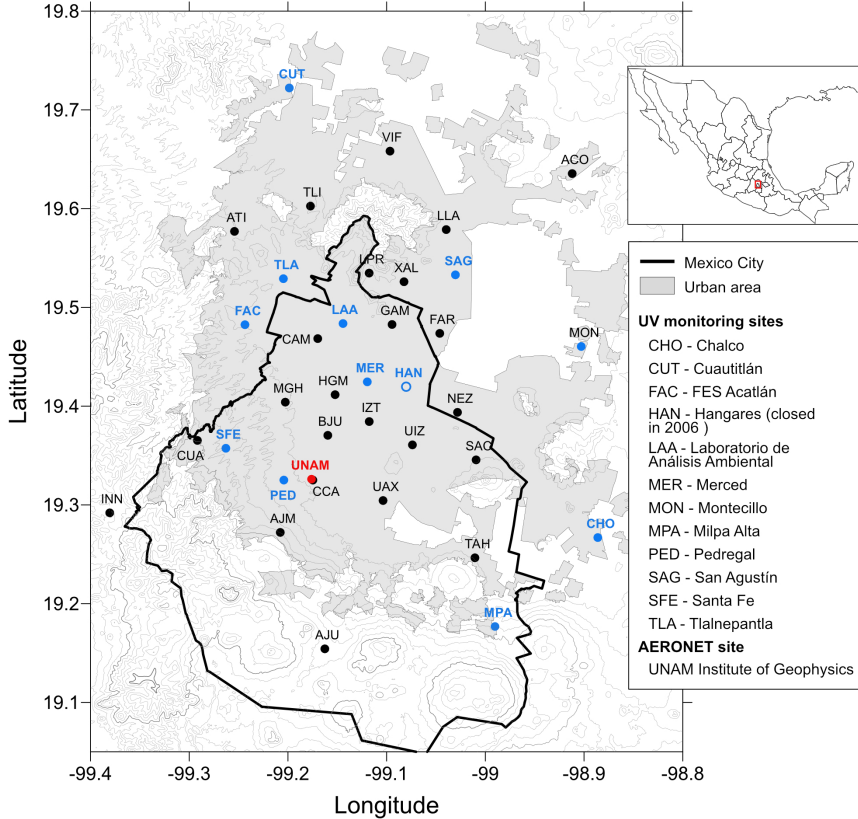


Figure 1: Map with the location of the SIMAT continuous monitoring stations over MCMA. Sites denoted by the blue solid dots correspond to SIMAT stations with UV measurements, while the black dots indicate SIMAT stations without UV measurements, the site indicated by an open blue dot represents a discontinued site, the red dot shows the location of the AERONET site. The location of Mexico City and the acronyms of the UV and AERONET site are shown at the upper and lower frames at the right respectively.

With the aim to explore the relationship between UVI and air pollutants levels, the hourly averages for ozone (O_3), carbon monoxide (CO), nitrogen dioxide (NO_2), sulfur dioxide (SO_2) and particle matter with diameter sizes $\leq 10 \mu m$ (PM_{10}), were downloaded from the SIMAT.³⁷ For purposes of assessing the influence on the UV Index at solar noon, only values obtained between 11h and 15h CST were considered for the trends analysis. Pollutant measurements are conducted by the SIMAT using regulatory-grade commercial instruments. Measurement principles include ultraviolet photometry (model 400E, Teledyne-API) for O_3 , chemiluminescence (model 200E, Teledyne-API) for NO_2 , UV fluorescence (model 100E, Teledyne API) for SO_2 , and infrared absorption (model 300E, Teledyne-API) for CO.

¹⁰⁴ The PM₁₀ continuous mass concentration was measured with Tapered Element Oscillating
¹⁰⁵ Microbalance (TEOM 1400AB or TEOM 1405 DF, Thermo Scientific) monitors. Gaseous
¹⁰⁶ pollutant levels are reported in ppb concentration units for O₃, SO₂ and NO₂, and in ppm
¹⁰⁷ for CO. Particulate matter mass concentration is reported in $\mu\text{g m}^{-3}$ at local conditions for
¹⁰⁸ temperature and pressure.

¹⁰⁹ Aerosol optical depth at 340 nm was obtained from the Institute of Geophysics of the
¹¹⁰ National Autonomous University of Mexico (UNAM). Measurements were conducted with
¹¹¹ a CIMEL sun photometer model CE-318, which is an automatic sun-sky-scanning spectral
¹¹² radiometer of the AErosol RObotic NETwork (AERONET³⁸). The data Product Level
¹¹³ 2.0 and 1.5 (only in 2019) were selected, and annual averages AOD₃₄₀ were calculated for
¹¹⁴ the period 2000-2019, except for the year 2011 which contained large data gaps and was
¹¹⁵ therefore not used. A previous study of the AOD behavior from 2000 to 2014 demonstrated
¹¹⁶ that data gaps did not significantly change the trends calculated for this.³⁹ Only 8% of the
¹¹⁷ data between the years 2014 and 2019 were missing. The largest data gap occurred in 2018
¹¹⁸ when the instrument was returned for calibration.

¹¹⁹ Satellite data

¹²⁰ The UV Index data derived from satellite-based measurements were used for comparing to the
¹²¹ ground-based measurements. These data were provided by the Ozone Monitoring Instrument
¹²² (OMI) on board of AURA-NASA satellite.⁴⁰ OMI is operated in cooperation between the
¹²³ Netherlands Agency for Aerospace Programmes (NIVR), the Finnish Meteorological Institute
¹²⁴ (FMI) and NASA. OMI performs observations over a geographical area of $13 \times 24\text{km}^2$ at
¹²⁵ nadir. For the coordinates (19.33°N, 99.18°W) and elevation (2268 m asl) of Mexico City,
¹²⁶ the satellite overpass time is between 19:00h - 21:00h UTC (20:00h - 22:00h CET). The
¹²⁷ OMI instrument measures reflected and backscattered radiances of the atmosphere-surface
¹²⁸ system at several UV wavelengths. The ozone column is estimated by differential absorption
¹²⁹ of several adjacent wavelengths in the O₃ Huggins band⁴¹ while clouds are estimated from

130 the reflectivity at a wavelength not affected by O₃ absorption (360 nm, Tanskanen et al. ⁴²).
131 A correction for absorbing aerosols is made using a global aerosol climatology ⁴³. The UV
132 Index used for Mexico City corresponds to values at local noon time and clear sky from
133 OMUVB Level 2 OVP data product, version 1.3 and collection 3.

134 TUV model

135 Calculations of the UV Index were also made with the Tropospheric Ultraviolet Visible (TUV
136 v5.3) model. ⁴⁴ The model atmosphere is represented by 80 vertical layers, each 1 km thick,
137 starting at the 2.24 km asl elevation of MCMA, and for which the first three km constitute
138 the atmospheric boundary layer (BL). ⁴⁵ The ozone profile above the BL is from the US
139 Standard Atmosphere, but rescaled to a value of 259.6 DU. Total ozone columns including
140 the BL contributions (of 13.7 DU in the year 2000 and 9.8 DU in 2019, see below) were
141 273.1 DU in 2000 and 269.2 DU in 2019, respectively. The climatological O₃ column for this
142 latitude and season is about 270 DU (plus or minus ca. 5 DU) so in good agreement with
143 the values used here.

144 Pollutants within the BL (including O₃) are assumed to be well mixed, in agreement with
145 observations from the MILAGRO field campaign that showed the disappearance of vertical
146 gradients in the profiles of gases ^{46,47} and aerosols ^{48,49} by late morning. The UV-absorbing
147 gases considered here are O₃, NO₂, and SO₂, specified in ppb.

148 BL aerosols are modeled by prescribing the AOD at 340 nm (from AERONET observa-
149 tions), scaled to other wavelengths inversely with wavelength (Angstrom coefficient = 1.0),
150 asymmetry factor of 0.7, and a single scattering albedo of 0.85 at UV wavelengths, following
151 the determinations made in Mexico City by Corr et al. ⁵⁰ and Palancar et al. ¹².

152 Above the atmospheric boundary layer, the model atmosphere was specified to be, NO₂,
153 or SO₂. In one sensitivity study, a total AOD of 0.7 was redistributed placing 0.2 in the free
154 troposphere (decreasing vertically with an exponential scale height of 4 km, and 0.5 remaining
155 in the BL). The calculated UVI differed by less than 1%. Thus, as long as the total AOD

₁₅₆ is known, knowledge of the exact vertical aerosol profile is not critical for ground-level UVI
₁₅₇ but would obviously affect the vertical structure of photolysis frequencies.

₁₅₈ Radiative transfer calculations were carried out with the pseudo-spherical 4-stream op-
₁₅₉ tion, at 1 nm steps between 280 and 400 nm.

₁₆₀ Results and Discussion

₁₆₁ Figure 2 shows the diurnal variation of the UVI for several specific cloud-free days, for
₁₆₂ different seasons and several locations (CHO, MER, MON, PED, SAG, SFE and TLA).
₁₆₃ UV Index calculated with the TUV model was used as reference of the behavior during
₁₆₄ clear sky days. According to the comparison of measurements minute by minute, the dates
₁₆₅ with prolonged fluctuations along the day were discarded. However, during the rainy period
₁₆₆ (from June to October) at least a brief episode of clouds, as shown at CHO station around
₁₆₇ noon in 13 June 2017. Peak values range from 8 during autumn/winter to above 12 in
₁₆₈ spring/summer, in correspondence to the respective December and June solstices. Although
₁₆₉ the stations are all within a 25 km radius, substantial differences among them are notable.
₁₇₀ Survey of the locations revealed that shadowing from nearby structures is not an issue. The
₁₇₁ good agreement in the morning, followed by more divergence in the afternoon, is consistent
₁₇₂ with the development of photo-chemical pollution hotspots during the day. Previous studies
₁₇₃ (e.g., Castro et al. ⁵¹ and Palancar et al. ¹²) have shown that surface UV radiation in Mexico
₁₇₄ City is attenuated significantly by aerosols. The measurements shown in Fig. 2 are consistent
₁₇₅ with this increasing pollution during the course of the day, with highest aerosol loading (and
₁₇₆ highest variability) attained in the afternoon. Further support for the role of pollution in
₁₇₇ suppressing the UVI comes from the observation made at the Santa Fe (SFE) site which in
₁₇₈ Fig. 2 are seen to be systematically higher, e.g. by over 10% in autumn afternoons, compared
₁₇₉ to the other stations. The SFE station is displaced to the west from the majority of the other
₁₈₀ stations, and remains in the outskirts. This site is also approximately 300 m higher than

181 Mexico City downtown, so that the cleaner atmosphere at SFE is a result of the station's
 182 location farther away from pollution sources, both horizontally and vertically.⁵² It is indeed
 183 expected to have higher values of the UVI, in agreement with the observations.

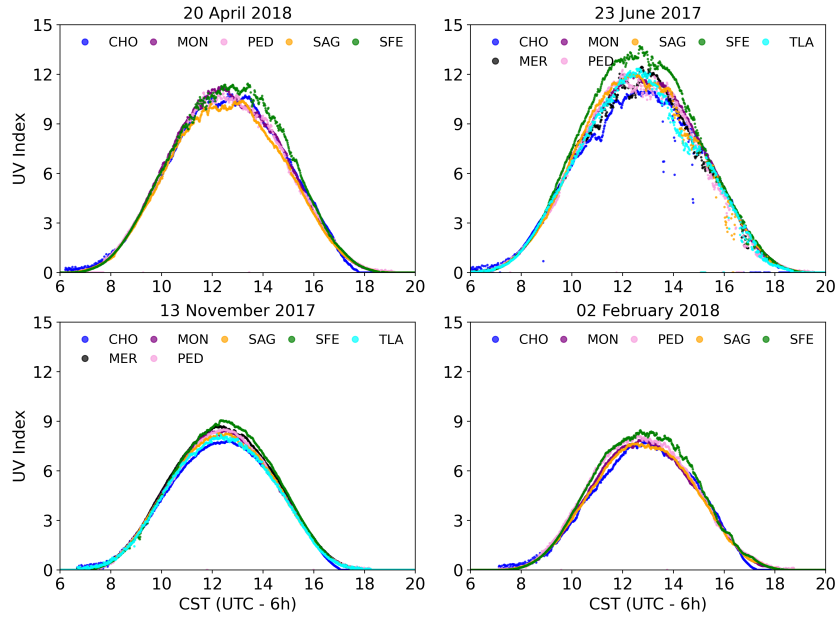


Figure 2: UV Index measurements at 1-minute resolution from several SIMAT stations within the MCMA under mostly cloudless conditions for representative days of the year.

184 The daily maximum UV Index of each station is denoted by UVI_{max} , these values were
 185 counted in the period 2000-2019. As shown in Figure 3, these values ranged from 1 to
 186 16, with a majority (61%) of the days experienced UVI_{max} values between 6 and 10, and
 187 remarkably few, less than 1%, in the 13-16 range. The lowest values are likely due to winter
 188 days with heavy cloud cover and low sun angles, and UV attenuation by pollutants could
 189 also be amplified under such conditions, due to longer photon path lengths at low sun and
 190 within clouds. The extreme sparsity of high UVI values remains surprising, and may be an
 191 indication of the rarity of extremely unpolluted days within the city.

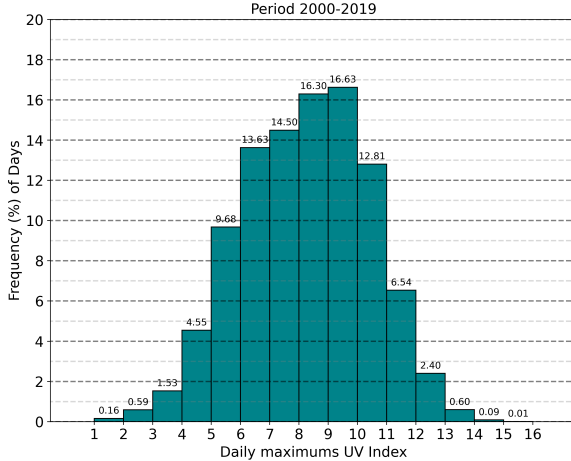


Figure 3: Frequency distribution of daily maximum UV Index values in Mexico City during 2000 -2019.

192 Similar patterns are found when considering the monthly average of the UVI_{max} values

193 as shown in Figure 4. The long-term averages present a seasonal variation (as in Fig. 2) that

194 follows approximately the cosine of the noontime solar zenith angle. Notably, values rarely

195 if ever exceed 12 (as in Fig. 3). The lowest average UVI (near 7) occurs in winter while

196 from March to August the values seem to be flattened in the range 10-11. The rather low

197 monthly UV Index values could be a consequence of the presence of clouds in the rainy season.

198 However, urban aerosol pollution sources, biomass burning for agriculture and wood cooking

199 also contribute to poor air quality between March-May⁵³. Using the maximum UVI_{max} from

200 all of stations every day (one daily point), the monthly averages (\overline{UVI}_m) were calculated

201 along the period 2000-2019 (except for June 2003 due to there were no measurements). Long

202 term trends in \overline{UVI}_m are shown in Figure 5. A clear upward trend is seen, with a slope for

203 the linear fit of 0.9%/year or +1.5 UVI units over the two decades.

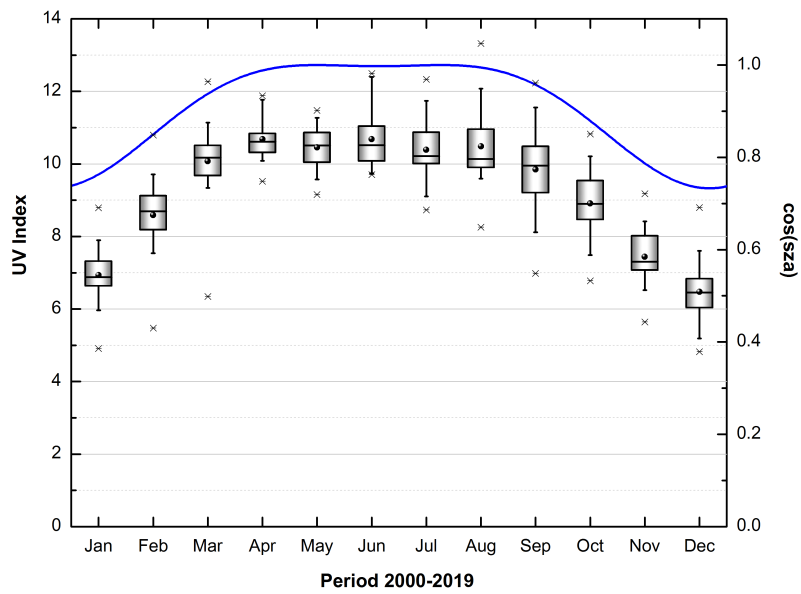


Figure 4: Boxplot of the monthly averages of the maximum UV Index values (black dot) in MCMA for the period 2000-2019: median (central bold line), interquartile range (box edges), 10% and 90% percentiles (the whiskers), the minimum and maximum values (asterisk) and the cosine of the solar zenith angle at solar noon (blue curve).

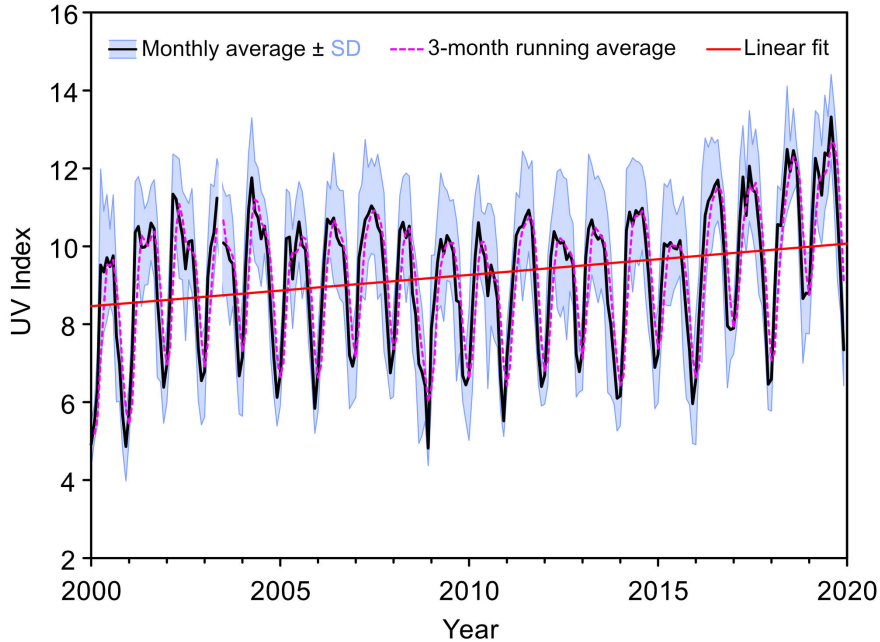


Figure 5: 3-month running average (violet segments curve) applied to monthly average UV Index (black line), the standard deviation (blue fill area) and linear fit (red line).

The UV Index computed from satellite-based observations over the period 2005-2019 is shown in Figure 6. The satellite-derived UVIs vary from 8 in winter to 16 in summer, these values being substantially higher than the ground-based observations (ca. 7 for winter and 11 for summer, see Fig. 4). For both datasets the maximum values are reached in June and July of each year. We hypothesize that this large difference between satellite-based estimation and ground-based observation of the UV index is due to the intense air pollution of Mexico City. A rather similar behavior was detected in Santiago city, Chile.⁵⁴ Although the OMI data are corrected for climatological aerosol absorption⁴³, this correction likely underestimates the absorption within the polluted Mexico City BL.

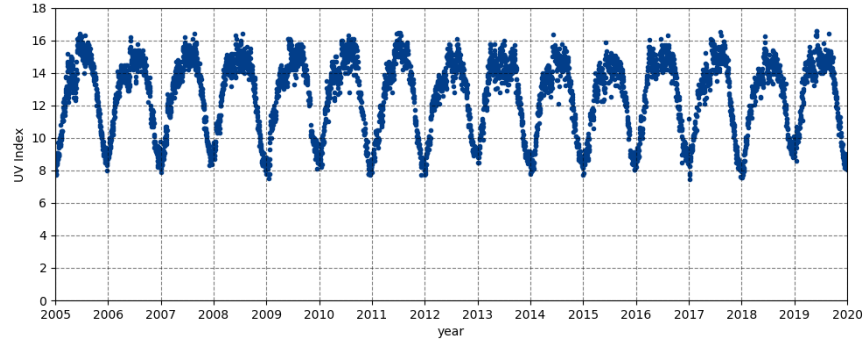


Figure 6: UV Index at solar noon for clear sky recorded by OMI-Aura/NIVR-FMI-NASA, from 2005 to 2019.

²¹³ Effect of pollutants on UV radiation

²¹⁴ Trends and averages in aerosol optical depth AOD_{340} and criteria pollutants PM_{10} , CO,
²¹⁵ NO_2 , O_3 and SO_2 observed at the SIMAT stations over 2000-2019, are shown in Figure 7
²¹⁶ and summarized in Table 2 together with the UVI_{max} . Similar trends in pollutants have
²¹⁷ been noted before⁵⁵⁻⁵⁷ and reflect the long-term success of emission reduction policies and
²¹⁸ programs.

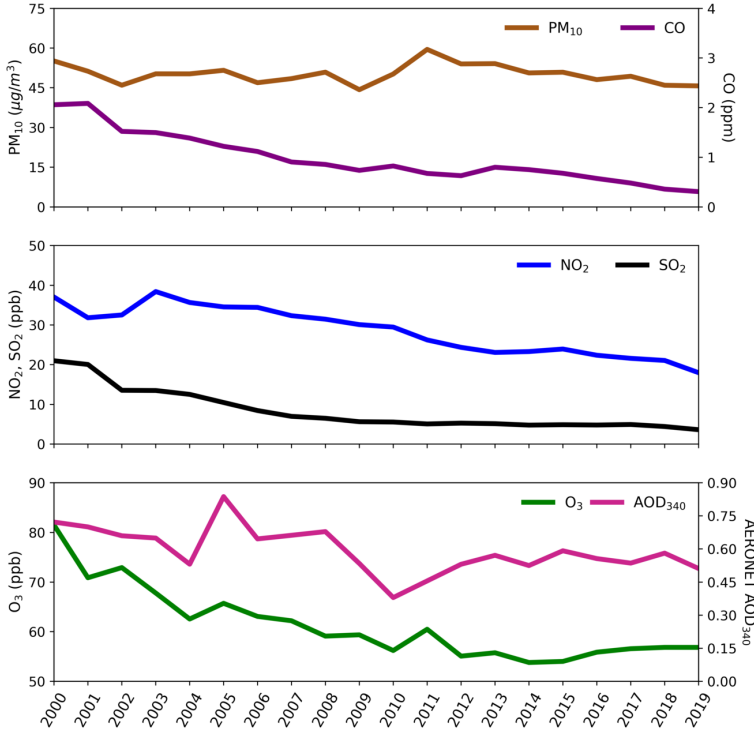


Figure 7: Air quality trends in MCMA for the period 2000-2019 from annual averages obtained between 11h to 15h CST every day: PM₁₀ (brown curve), CO (purple curve), NO₂ (blue curve), SO₂(black curve), O₃ (green curve) and AOD₃₄₀ (pink curve).

Table 2: UV Index and criteria pollutants: the absolute change per year for the period 2000-2019, averages in units of $\mu\text{g}/\text{m}^3$ (PM₁₀), ppm (CO), ppb (SO₂, NO₂ and O₃), dimensionless (UV Index and AOD₃₄₀) and annual percentage change (%/year).

Variable	$\frac{\text{absolutechange}}{\text{year}}$	Avg _{2000–2019}	$\Delta(\%/\text{year})$
UVI	0.08	9.2	0.9
PM ₁₀	-0.10	50.2	-0.2
CO	-0.08	1.0	-8.2
NO ₂	-0.96	28.6	-3.4
O ₃	-1.05	61.3	-1.7
AOD ₃₄₀	-0.01	0.6	-1.6
SO ₂	-0.76	8.4	-9.1

The observed changes in the concentrations of these air pollutants have significant implications for surface UV radiation, as can be demonstrated with the TUV radiative transfer model. Table 3 summarizes UVI values for the June-July time period, estimated by the three

222 methods: OMI satellite-derived UVI, SIMAT ground-based observations, and TUV model-
 223 ing using air pollution estimates. Two groups of values can be readily identified: (1) SIMAT
 224 daily record values, OMI with or without BL aerosols, and TUV for very clean conditions, all
 225 with UVI values around 15-16; and (2) the average of daily maxima of SIMAT observations
 226 and TUV UVI results using MCMA pollutants as input. Note that SIMAT and TUV values
 227 are in good agreement for both 2018-2019 and 2000-2001 and are considerably lower than for
 228 case (1). Compared to the OMI estimate that included the climatological aerosol correction
 229 (15.3), observed SIMAT values were lower by 35% in 2000 and by 20% in 2019. Similarly,
 230 TUV values were 35% lower in 2000 and 22% lower in 2019 relative to the TUV values of
 231 15.6 for a pristine atmosphere.

Table 3: UVI maxima for June-July: averages and standard deviation from ground-based data for the years 2018-2019 and 2000-2001. UVI maximum value reached in the period 2000-2019 for UVI ground-based and the same for satellite in the period 2005-2019. TUV calculations for different conditions.

Conditions for estimation in June-July	UV Index
SIMAT average maxima 2000-2001	9.9 ± 1.2
SIMAT average maxima 2018-2019	12.3 ± 1.3
SIMAT maximum value reached in period 2000-2019	15.0
OMI maximum value reached in period 2005-2019, not corrected for BL aerosols	16.6
TUV "zero" pollution	16.1
AOD 0, O ₃ 0 ppb, NO ₂ 0 ppb, SO ₂ 0 ppb	
TUV pristine pollution	15.6
AOD 0.05, O ₃ 10 ppb, NO ₂ 0 ppb, SO ₂ 0 ppb	
TUV 2019:	12.1
AOD 0.5, O ₃ 50 ppb, NO ₂ 20 ppb, SO ₂ 1 ppb	
TUV 2000:	10.2
AOD 0.7, O ₃ 70 ppb, NO ₂ 40 ppb, SO ₂ 20 ppb	

232 The agreement between SIMAT observations and TUV model estimates is excellent but
 233 also probably a bit fortuitous. Clouds on average reduce the irradiance impinging on the
 234 surface, but scattering from them can also cause transient enhancements (these are only
 235 possible if the disk of the Sun is visible) that could be recorded as daily maxima – with
 236 cancellation between these cloud effects resulting in improved agreement with the cloud-free

²³⁷ model. We cannot exclude that some of the observed trend in UVI is due to changes in cloud
²³⁸ cover. However, the modeled fractional UVI reductions due to pollutants, shown in Table 3,
²³⁹ are in such good agreement with the observed UVI reductions, that a compelling case can
²⁴⁰ be made for a dominant role of air pollutants in the long-term UVI trends.

²⁴¹ Table 4 shows the contributions to UVI reductions from individual pollutants. Aerosols
²⁴² are seen to be the major factor in both time periods, followed by O₃, NO₂, and SO₂. The
²⁴³ 2000-2019 UVI increase results in comparable proportions from less aerosols, less SO₂, and
²⁴⁴ the combined reductions in O₃ and NO₂.

²⁴⁵ Comparable UV reductions, of 30-40% due to aerosols, were reported by Panicker et al.¹¹
²⁴⁶ over Pune, India from April 2004 to March 2005, with sensitivity coefficients (i.e. change in
²⁴⁷ UVI per unit change in AOD) similar to those found here in Table 3.

²⁴⁸ Comparisons of OMI with ground-based UV measurements have been reviewed recently
²⁴⁹ by Zhang et al.⁵⁸ and Vitt et al.⁵⁹. OMI-derived UV generally overestimates ground-level
²⁵⁰ measurements by 1-10% in relatively clean conditions (e.g. rural U.S), by 10-30% in Southern
²⁵¹ Europe and by 40% or more in Santiago, Chile⁵⁴ and Thailand⁶⁰. The overestimations appear
²⁵² related in large part to incomplete accounting of UV absorption by BL aerosol, although
²⁵³ other factors such as the correction to solar noon may also introduce some bias.⁵⁸ Over
²⁵⁴ Europe, ground-based UVI observations for several decades are systematically lower than
²⁵⁵ those estimated from satellites even after consideration of climatological aerosol distributions,
²⁵⁶ showing the importance of local pollution not resolved from space.⁵⁹ However, difference
²⁵⁷ between satellite-derived and ground-based UVI was less than 1.0 UVI units in over 90% of
²⁵⁸ the cases, in contrast to the difference of 3-5 units found for Mexico City (Table 3).

²⁵⁹ UV reductions by air pollutants are expected to be most severe near the surface, while
²⁶⁰ chemical reactions leading to photochemical smog occur throughout the vertical extent of the
²⁶¹ BL. Figure 8 shows the vertical profiles of photolysis coefficients (the reciprocals of photolytic
²⁶² lifetimes) computed with the TUV model, for two key reactions, the photolysis of O₃ to yield
²⁶³ excited oxygen atoms O(1D), and the photolysis of NO₂. In the absence of optically active

264 pollutants, these coefficients would be nearly independent of altitude in the BL. However,
 265 the presence of pollutants leads to a strong decrease toward the surface, with notably more
 266 severe reductions in 2000 compared to 2019. While the specific values shown in the figure
 267 are only illustrative for typical conditions, routine daily air quality modeling should carefully
 268 account for the long term variations in these photolysis coefficients.

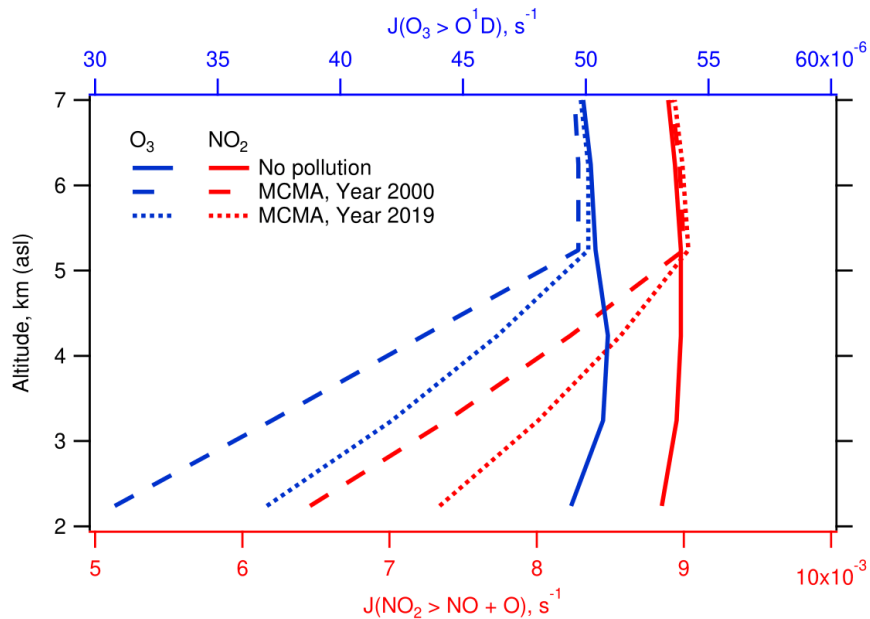


Figure 8: Vertical profiles of the photolysis coefficients for the reaction $O_3+h\nu \rightarrow O(1D)+O_2$ (top axis, blue) $NO_2+h\nu \rightarrow O+NO$ (bottom axis, red) for zero pollution (solid) and Mexico City in the years 2000 (dashed) and 2019 (dotted)

269 An issue that is beginning to gain relevance in radiative balance models is the influence
 270 of a group of organic compounds known as “brown carbon” that are capable of strongly
 271 absorbing in the UV region.⁶¹ Some of these compounds are related to emissions from local
 272 and regional wildfires.⁶² Mexico City is frequently exposed to regional fire smoke transport
 273 during the dry part of the year (November to May)⁶³, which sporadically modify the optical
 274 properties of the aerosols.⁶⁴ This could partly explain the relatively minor reductions in
 275 PM₁₀ (see Fig. 7), compared to the larger reductions of CO, NO₂, and O₃ that are more
 276 directly related to urban activities, as well as some of the seasonal asymmetry seen in Fig.
 277 3.

278 The UVI is specific to wavelengths mainly in the 300-320 nm range, and so the question
 279 remains whether these results can be applied at longer UV wavelengths, e.g. those important
 280 for NO₂ photolysis (<420 nm). Absorption by SO₂ and O₃ vanishes for wavelengths larger
 281 than about 330 nm, while NO₂ photolysis is mostly driven by UV-A radiation and typical
 282 aerosols optical depth decrease with wavelength. These changes can easily be modeled, but
 283 unfortunately far fewer measurements of these longer wavelengths are available in Mexico
 284 City or elsewhere.

285 Two decades of observations in Mexico City demonstrate unequivocally that air pollution
 286 reduces UV radiation at the ground. The ground-based observations are well below values
 287 derived from satellite-based observations. Although ideally both data sets should match,
 288 the satellite has a limitation to seeing boundary layer absorbers. When typical values of
 289 the pollutants: aerosols, tropospheric ozone, and to a lesser extent NO₂ and SO₂, are in-
 290 cluded in a model (e.g. TUV), the differences between satellite-derived and ground-based
 291 measured values are explained and can be attributed quantitatively to individual observed
 292 pollutants. Long term improvements in air quality over the last two decades, are accompa-
 293 nied by statistically significant increases in the observed UVI, again in good agreement with
 294 the model-predicted changes.

Table 4: Contributions of individual pollutants to UV Index changes. (a) Values used one at the time, with the others held at zero. (b) UVI deviation from the zero-pollution value of 16.1 (from Table 3). (c) 2000-2019 UVI change due to changes in each pollutant.

Pollutant	Year 2000		Year 2019		2000-2019 (c)
	poll. level (a)	UVI (b)	poll. level	UVI	
AOD	0.7	-3.7	0.5	-2.7	1.0
O ₃ ppb (DU)	70 (14)	-1.4	50 (10)	-1.0	0.4
NO ₂ ppb	40	-0.9	20	-0.5	0.4
SO ₂ ppb	30	-0.8	1	-0.04	0.8

295 The reductions in surface UV radiation with respect to an ideally clear atmosphere –
 296 by nearly 40% in 2000 and still 20% in 2020 – are large, both within the context of hu-
 297 man UV exposure and air quality mitigation. In urban areas where ozone production scales

298 proportionally with UV levels and with volatile organic compound (VOC) emissions (the
299 VOC-limited regime), a 10% increase in BL average photolysis rates means that VOC emis-
300 sions will need to be reduced by 10% to meet the same goals, or else successful reductions
301 in aerosols would lead to unwanted UV-driven increases in O₃. Such UV changes must be
302 considered carefully in air quality mitigation strategies. For human exposure, a 20% increase
303 in UV irradiances over two decades should be seen as a non-negligible public health issue
304 requiring some reassessment of preventive behaviors to minimize the risk of skin cancer,
305 cataract, and other UV-related health effects. The efforts that Mexico City has made to
306 improve air quality have reduced levels of most air pollutants. Nevertheless, they caused an
307 increase in UV radiation that reaches the surface.

308 Finally, based on our results, the solar radiation monitoring network could be improved
309 by adding observation sites within or close to the Valley of Mexico, with minor influences of
310 the urban plume (e. g., Amecameca; latitude: 19.13°N, longitude: 99.76°W, elevation: 2420
311 m asl), and the complementing of sensors in existing monitoring sites that are at elevations
312 above the urban boundary layer like Ajusco (AJU, elevation: 2953 m asl) or Instituto de
313 Investigaciones Nucleares (INN, elevation: 3082 m asl). These sites would provide valuable
314 observations to assess quantitatively the effects of urban pollution on solar radiation levels.

315 Acknowledgement

316 We wish to acknowledge the staff of SIMAT, from the Secretariat of Environment, for the
317 data and the continuous assistance during the realization of this project. Adriana Ipiña would
318 like to extend her thanks to Dirección General de Personal Académico, Universidad Nacional
319 Autónoma de México (DGAPA-UNAM) for the postdoctoral fellowship at Centro de Ciencias
320 de la Atmósfera of the UNAM. Rubén D Piacentini wishes to thank CONICET and National
321 University of Rosario, Argentina, for their partial support to the present work. The National
322 Center for Atmospheric Research is sponsored by the National Science Foundation.

323 **References**

- 324 (1) Taylor, H. R.; West, S. K.; Rosenthal, F. S.; Muñoz, B.; Newland, H. S.; Abbey, H.;
325 Emmett, E. A. Effect of Ultraviolet Radiation on Cataract Formation. *New England
326 Journal of Medicine* **1988**, *319*, 1429–1433.
- 327 (2) Varotsos, C.; Feretis, E. Health effects on human eye resulting from the increased
328 ambient solar ultraviolet radiation. *Toxicological & Environmental Chemistry* **1997**,
329 *61*, 43–68.
- 330 (3) Lucas, R. M.; Yazar, S.; Young, A. R.; Norval, M.; de Gruijl, F. R.; Takizawa, Y.;
331 Rhodes, L. E.; Sinclair, C. A.; Neale, R. E. Human health in relation to exposure to solar
332 ultraviolet radiation under changing stratospheric ozone and climate. *Photochemical &
333 Photobiological Sciences* **2019**, *18*, 641–680.
- 334 (4) Leighton, P. A. *Photochemistry of Air Pollution*; Elsevier, 1961; pp v–vi.
- 335 (5) Seinfeld, J. H.; Pandis, S. N.; Noone, K. Atmospheric Chemistry and Physics: From
336 Air Pollution to Climate Change. *Physics Today* **1998**, *51*, 88–90.
- 337 (6) Finlayson-Pitts, B. J.; Pitts, J. N. *Chemistry of the Upper and Lower Atmosphere*;
338 Academic Press, 2000; pp xvii–xviii.
- 339 (7) Liu, S. C.; McKeen, S. A.; Madronich, S. Effect of anthropogenic aerosols on biologically
340 active ultraviolet radiation. *Geophysical Research Letters* **1991**, *18*, 2265–2268.
- 341 (8) Sabziparvar, A. A.; Forster, P. M. F.; Shine, K. P. Changes in ultraviolet radiation due
342 to stratospheric and tropospheric ozone changes since preindustrial times. *Journal of
343 Geophysical Research: Atmospheres* **1998**, *103*, 26107–26113.
- 344 (9) Madronich, S.; Wagner, M.; Groth, P. Influence of Tropospheric Ozone Control on
345 Exposure to Ultraviolet Radiation at the Surface. *Environmental Science & Technology*
346 **2011**, *45*, 6919–6923.

- 347 (10) McKenzie, R. L.; Weinreis, C.; Johnston, P. V.; Liley, B.; Shiona, H.; Kotkamp, M.;
348 Smale, D.; Takegawa, N.; Kondo, Y. Effects of urban pollution on UV spectral irradi-
349 ances. *Atmospheric Chemistry and Physics* **2008**, *8*, 5683–5697.
- 350 (11) Panicker, A. S.; Pandithurai, G.; Takamura, T.; Pinker, R. T. Aerosol effects in the
351 UV-B spectral region over Pune an urban site in India. *Geophysical Research Letters*
352 **2009**, *36*, L10802 1–5.
- 353 (12) Palancar, G. G.; Lefer, B. L.; Hall, S. R.; Shaw, W. J.; Corr, C. A.; Herndon, S. C.;
354 Slusser, J. R.; Madronich, S. Effect of aerosols and NO₂ concentration on ultraviolet
355 actinic flux near Mexico City during MILAGRO: measurements and model calculations.
356 *Atmospheric Chemistry and Physics* **2013**, *13*, 1011–1022.
- 357 (13) Bais, A. F.; McKenzie, R. L.; Bernhard, G.; Aucamp, P. J.; Ilyas, M.; Madronich, S.;
358 Tourpali, K. Ozone depletion and climate change: impacts on UV radiation. *Photo-
359 chemical & Photobiological Sciences* **2015**, *14*, 19–52.
- 360 (14) Hollaway, M.; Wild, O.; Yang, T.; Sun, Y.; Xu, W.; Xie, C.; Whalley, L.; Slater, E.;
361 Heard, D.; Liu, D. Photochemical impacts of haze pollution in an urban environment.
362 *Atmospheric Chemistry and Physics* **2019**, *19*, 9699–9714.
- 363 (15) Li, K.; Jacob, D. J.; Liao, H.; Shen, L.; Zhang, Q.; Bates, K. H. Anthropogenic drivers
364 of 2013–2017 trends in summer surface ozone in China. *Proceedings of the National
365 Academy of Sciences* **2018**, *116*, 422–427.
- 366 (16) Wang, Y.; Gao, W.; Wang, S.; Song, T.; Gong, Z.; Ji, D.; Wang, L.; Liu, Z.; Tang, G.;
367 Huo, Y.; Tian, S.; Li, J.; Li, M.; Yang, Y.; Chu, B.; Petäjä, T.; Kerminen, V.-M.;
368 He, H.; Hao, J.; Kulmala, M. et al. *Contrasting trends of PM2.5 and surface-ozone
369 concentrations in China from 2013 to 2017*; Oxford University Press (OUP), 2020;
370 Vol. 7; pp 1331–1339.

- 371 (17) Wang, W.; Li, X.; Shao, M.; Hu, M.; Zeng, L.; Wu, Y.; Tan, T. The impact of aerosols
372 on photolysis frequencies and ozone production in Beijing during the 4-year period
373 2012–2015. *Atmospheric Chemistry and Physics* **2019**, *19*, 9413–9429.
- 374 (18) Gao, J.; Li, Y.; Zhu, B.; Hu, B.; Wang, L.; Bao, F. What have we missed when studying
375 the impact of aerosols on surface ozone via changing photolysis rates? *Atmospheric*
376 *Chemistry and Physics* **2020**, *20*, 10831–10844.
- 377 (19) Ma, X.; Huang, J.; Zhao, T.; Liu, C.; Zhao, K.; Xing, J.; Xiao, W. Rapid increase in
378 summer surface ozone over the North China Plain during 2013–2019: a side effect of
379 particulate matters reduction control? *Atmospheric Chemistry and Physics* **2021**, *21*,
380 1–16.
- 381 (20) Bauwens, M.; Compernolle, S.; Stavrakou, T.; Müller, J.-F.; Gent, J.; Eskes, H.; Lev-
382 elt, P. F.; A, R.; Veefkind, J. P.; Vlietinck, J.; Yu, H.; Zehner, C. Impact of coronavirus
383 outbreak on NO₂ pollution assessed using TROPOMI and OMI observations. **2020**,
384 *47*, e2020GL087978.
- 385 (21) Venter, Z. S.; Aunan, K.; Chowdhury, S.; Lelieveld, J. COVID-19 lockdowns cause
386 global air pollution declines. *Proceedings of the National Academy of Sciences* **2020**,
387 *117*, 18984–18990.
- 388 (22) Shi, X.; Brasseur, G. P. The Response in Air Quality to the Reduction of Chinese
389 Economic Activities During the COVID-19 Outbreak. *Geophysical Research Letters*
390 **2020**, *47*, e2020GL088070.
- 391 (23) Le, T.; Wang, Y.; Liu, L.; Yang, J.; Yung, Y. L.; Li, G.; Seinfeld, J. H. Unexpected air
392 pollution with marked emission reductions during the COVID-19 outbreak in China.
393 *Science* **2020**, *369*, 702–706.
- 394 (24) Red Automática de Monitoreo Atmosférico (RAMA). <http://www.aire.cdmx.gob.mx/descargas/datos/excel/RAMA.xls.pdf>.

- 396 (25) Doran, J. C.; Abbott, S.; Archuleta, J.; Bian, X.; Chow, J.; Coulter, R. L.; de Wekker, S.
397 F. J.; Edgerton, S.; Elliott, S.; Fernandez, A.; Fast, J. D.; Hubbe, J. M.; King, C.; Lan-
398 gley, D.; Leach, J.; Lee, J. T.; Martin, T. J.; Martinez, D.; Martinez, J. L.; Mercado, G.
399 et al. The IMADA-AVER Boundary Layer Experiment in the Mexico City Area. *Bulletin of the American Meteorological Society* **1998**, *79*, 2497–2508.
- 400
401 (26) Molina, L. T.; Kolb, C. E.; de Foy, B.; Lamb, B. K.; Brune, W. H.; Jimenez, J. L.;
402 Ramos-Villegas, R.; Sarmiento, J.; Paramo-Figueroa, V. H.; Cardenas, B.; Gutierrez-
403 Avedoy, V.; Molina, M. J. Air quality in North America's most populous city – overview
404 of the MCMA-2003 campaign. *Atmospheric Chemistry and Physics* **2007**, *7*, 2447–2473.
- 405
406 (27) Molina, L. T.; Madronich, S.; Gaffney, J. S.; Apel, E.; de Foy, B.; Fast, J.; Ferrare, R.;
407 Herndon, S.; Jimenez, J. L.; Lamb, B.; Osornio-Vargas, A. R.; Russell, P.; Schauer, J. J.;
408 Stevens, P. S.; Volkamer, R.; Zavala, M. An overview of the MILAGRO 2006 Campaign:
409 Mexico City emissions and their transport and transformation. *Atmospheric Chemistry
and Physics* **2010**, *10*, 8697–8760.
- 410
411 (28) Jazcilevich, A. D.; García, A. R.; Caetano, E. Locally induced surface air confluence
412 by complex terrain and its effects on air pollution in the valley of Mexico. *Atmospheric
Environment* **2005**, *39*, 5481–5489.
- 413
414 (29) Tie, X.; Madronich, S.; Li, G.; Ying, Z.; Zhang, R.; Garcia, A. R.; Lee-Taylor, J.; Liu, Y.
415 Characterizations of chemical oxidants in Mexico City: A regional chemical dynamical
model (WRF-Chem) study. *Atmospheric Environment* **2007**, *41*, 1989–2008.
- 416
417 (30) Zhang, Y.; Dubey, M. K.; Olsen, S. C.; Zheng, J.; Zhang, R. Comparisons of
418 WRF/Chem simulations in Mexico City with ground-based RAMA measurements dur-
ing the 2006-MILAGRO. *Atmospheric Chemistry and Physics* **2009**, *9*, 3777–3798.
- 419 (31) Zavala, M.; Brune, W. H.; Velasco, E.; Retama, A.; Cruz-Alavez, L. A.; Molina, L. T.

- 420 Changes in ozone production and VOC reactivity in the atmosphere of the Mexico City
421 Metropolitan Area. *Atmospheric Environment* **2020**, *238*, 117747.
- 422 (32) WHO,; WMO,; UNEP,; ICNIRP, *Global solar UV index : a practical guide*; 2002; pp A
423 joint recommendation of the World Health Organization, World Meteorological Orga-
424 nization, United Nations Environment Programme, and the International Commission
425 on Non-Ionizing Radiation Protection.
- 426 (33) Webb, A. R.; Slaper, H.; Koepke, P.; Schmalwieser, A. W. Know Your Standard: Clari-
427 fying the CIE Erythema Action Spectrum. *Photochemistry and Photobiology* **2011**, *87*,
428 483–486.
- 429 (34) Whiteman, C. D.; Zhong, S.; Bian, X.; Fast, J. D.; Doran, J. C. Boundary layer evo-
430 lution and regional-scale diurnal circulations over the and Mexican plateau. *Journal of*
431 *Geophysical Research: Atmospheres* **2000**, *105*, 10081–10102.
- 432 (35) Fast, J. D.; de Foy, B.; Rosas, F. A.; Caetano, E.; Carmichael, G.; Emmons, L.;
433 McKenna, D.; Mena, M.; Skamarock, W.; Tie, X.; Coulter, R. L.; Barnard, J. C.;
434 Wiedinmyer, C.; Madronich, S. A meteorological overview of the MILAGRO field cam-
435 paigns. *Atmospheric Chemistry and Physics* **2007**, *7*, 2233–2257.
- 436 (36) Carreón-Sierra, S.; Salcido, A.; Castro, T.; Celada-Murillo, A.-T. Cluster Analysis of
437 the Wind Events and Seasonal Wind Circulation Patterns in the Mexico City Region.
438 *Atmosphere* **2015**, *6*, 1006–1031.
- 439 (37) Sistema de Monitoreo Atmosférico,Ciudad de México. [http://www.aire.cdmx.gob.
440 mx/default.php?opc=%27aKBhnml=%27&opcion=Zg](http://www.aire.cdmx.gob.mx/default.php?opc=%27aKBhnml=%27&opcion=Zg), Accessed on Wed, December 02,
441 2020.
- 442 (38) Holben, B.; Eck, T.; Slutsker, I.; Tanré, D.; Buis, J.; Setzer, A.; Vermote, E.; Reagan, J.;
443 Kaufman, Y.; Nakajima, T.; Lavenu, F.; Jankowiak, I.; Smirnov, A. AERONET—A

- 444 Federated Instrument Network and Data Archive for Aerosol Characterization. *Remote*
445 *Sensing of Environment* **1998**, *66*, 1–16.
- 446 (39) Carabali, G.; Estévez, H. R.; Valdés-Barrón, M.; Bonifaz-Alfonzo, R.; Riveros-
447 Rosas, D.; Velasco-Herrera, V. M.; Vázquez-Gálvez, F. A. Aerosol climatology over
448 the Mexico City basin: Characterization of optical properties. *Atmospheric Research*
449 **2017**, *194*, 190–201.
- 450 (40) NASA EOS/Aura Validation Data Center (AVDC) - Correlative data, Field of
451 View Predictions, Data Subsets, GEOMS, DCIO. [https://avdc.gsfc.nasa.gov/pub/
452 most_popular/overpass/OMI/](https://avdc.gsfc.nasa.gov/pub/most_popular/overpass/OMI/).
- 453 (41) Veefkind, J. P.; de Haan, J. F.; Brinksma, E. J.; Kroon, M.; Levelt, P. F. Total Ozone
454 From the Ozone Monitoring Instrument (OMI) Using the DOAS Technique. *IEEE*
455 *Transactions on Geoscience and Remote Sensing* **2006**, *44*, 1239–1244.
- 456 (42) Tanskanen, A.; Lindfors, A.; Määttä, A.; Krotkov, N.; Herman, J.; Kaurola, J.;
457 Koskela, T.; Lakkala, K.; Fioletov, V.; Bernhard, G.; McKenzie, R.; Kondo, Y.;
458 O'Neill, M.; Slaper, H.; den Outer, P.; Bais, A. F.; Tamminen, J. Validation of daily ery-
459 themal doses from Ozone Monitoring Instrument with ground-based UV measurement
460 data. *Journal of Geophysical Research: Atmospheres* **2007**, *112*, D24S44 1–15.
- 461 (43) Arola, A.; Kazadzis, S.; Lindfors, A.; Krotkov, N.; Kujanpää, J.; Tamminen, J.;
462 Bais, A.; di Sarra, A.; Villaplana, J. M.; Brogniez, C.; Siani, A. M.; Janouch, M.;
463 Weihs, P.; Webb, A.; Koskela, T.; Kouremeti, N.; Meloni, D.; Buchard, V.; Auriol, F.;
464 Ialongo, I. et al. A new approach to correct for absorbing aerosols in OMI UV. *Geo-
465 physical Research Letters* **2009**, *36*, L22805 1–5.
- 466 (44) Madronich, S. Intercomparison of NO₂ photodissociation and U.V. Radiometer Mea-
467 surements. *Atmospheric Environment* **1987**, *21*, 569–578.

- 468 (45) Shaw, W. J.; Pekour, M. S.; Coulter, R. L.; Martin, T. J.; Walters, J. T. The daytime
469 mixing layer observed by radiosonde profiler, and lidar during MILAGRO. *Atmospheric*
470 *Chemistry and Physics Discussions* **2007**, *7*, 15025–15065.
- 471 (46) Velasco, E.; Márquez, C.; Bueno, E.; Bernabé, R. M.; Sánchez, A.; Fentanes, O.; Wöhrn-
472 schimmel, H.; Cárdenas, B.; Kamilla, A.; Wakamatsu, S.; Molina, L. T. Vertical dis-
473 tribution of ozone and VOCs in the low boundary layer of Mexico City. *Atmospheric*
474 *Chemistry and Physics* **2008**, *8*, 3061–3079.
- 475 (47) Greenberg, J.; Guenther, A.; Turnipseed, A. Tethered balloon-based soundings of ozone
476 aerosols, and solar radiation near Mexico City during MIRAGE-MEX. *Atmospheric*
477 *Environment* **2009**, *43*, 2672–2677.
- 478 (48) Rogers, R. R.; Hair, J. W.; Hostetler, C. A.; Ferrare, R. A.; Obland, M. D.; Cook, A. L.;
479 Harper, D. B.; Burton, S. P.; Shinozuka, Y.; McNaughton, C. S.; Clarke, A. D.; Re-
480 demann, J.; Russell, P. B.; Livingston, J. M.; Kleinman, L. I. NASA LaRC airborne
481 high spectral resolution lidar aerosol measurements during MILAGRO: observations
482 and validation. *Atmospheric Chemistry and Physics* **2009**, *9*, 4811–4826.
- 483 (49) Lewandowski, P. A.; Eichinger, W. E.; Holder, H.; Prueger, J.; Wang, J.; Kleinman, L. I.
484 Vertical distribution of aerosols in the vicinity of Mexico City during MILAGRO-2006
485 Campaign. *Atmospheric Chemistry and Physics* **2010**, *10*, 1017–1030.
- 486 (50) Corr, C. A.; Krotkov, N.; Madronich, S.; Slusser, J. R.; Holben, B.; Gao, W.; Flynn, J.;
487 Lefer, B.; Kreidenweis, S. M. Retrieval of aerosol single scattering albedo at ultraviolet
488 wavelengths at the T1 site during MILAGRO. *Atmospheric Chemistry and Physics*
489 **2009**, *9*, 5813–5827.
- 490 (51) Castro, T.; Madronich, S.; Rivale, S.; Muhlia, A.; Mar, B. The influence of aerosols on
491 photochemical smog in Mexico City. *Atmospheric Environment* **2001**, *35*, 1765–1772.
- 492 (52) SEDEMA, *Calidad del aire en la Ciudad de México, Informe 2017*; 2018.

- 493 (53) Retama, A.; Baumgardner, D.; Raga, G. B.; McMeeking, G. R.; Walker, J. W. Sea-
494 sonal and diurnal trends in black carbon properties and co-pollutants in Mexico City.
495 *Atmospheric Chemistry and Physics* **2015**, *15*, 9693–9709.
- 496 (54) Cabrera, S.; Ipiña, A.; Damiani, A.; Cordero, R. R.; Piacentini, R. D. UV index values
497 and trends in Santiago Chile (33.5°S) based on ground and satellite data. *Journal of*
498 *Photochemistry and Photobiology B: Biology* **2012**, *115*, 73–84.
- 499 (55) Parrish, D. D.; Singh, H. B.; Molina, L.; Madronich, S. Air quality progress in North
500 American megacities: A review. *Atmospheric Environment* **2011**, *45*, 7015–7025.
- 501 (56) Secretaría del Medio Ambiente de la Ciudad de México, *Calidad del aire en la Ciudad*
502 *de México, informe 2017*; 2018; pp 1–160.
- 503 (57) Molina,; Velasco,; Retama,; Zavala, Experience from Integrated Air Quality Manage-
504 ment in the Mexico City Metropolitan Area and Singapore. *Atmosphere* **2019**, *10*,
505 512.
- 506 (58) Zhang, H.; Wang, J.; García, L. C.; Zeng, J.; Dennhardt, C.; Liu, Y.; Krotkov, N. A.
507 Surface erythemal UV irradiance in the continental United States derived from ground-
508 based and OMI observations: quality assessment trend analysis and sampling issues.
509 *Atmospheric Chemistry and Physics* **2019**, *19*, 2165–2181.
- 510 (59) Vitt, R.; Laschewski, G.; Bais, A.; Diémoz, H.; Fountoulakis, I.; Siani, A.-M.;
511 Matzarakis, A. UV-Index Climatology for Europe Based on Satellite Data. *Atmosphere*
512 **2020**, *11*, 727.
- 513 (60) Janjai, S.; Wisitsirikun, S.; Buntoung, S.; Pattarapanitchai, S.; Wattan, R.; Masiri, I.;
514 Bhattarai, B. K. Comparison of UV index from Ozone Monitoring Instrument (OMI)
515 with multi-channel filter radiometers at four sites in the tropics: effects of aerosols and
516 clouds. *International Journal of Climatology* **2013**, *34*, 453–461.

- 517 (61) Laskin, A.; Laskin, J.; Nizkorodov, S. A. Chemistry of Atmospheric Brown Carbon.
- 518 *Chemical Reviews* **2015**, *115*, 4335–4382.
- 519 (62) Gadhavi, H.; Jayaraman, A. Absorbing aerosols: contribution of biomass burning and
- 520 implications for radiative forcing. *Annales Geophysicae* **2010**, *28*, 103–111.
- 521 (63) Rios, B.; Raga, G. B. Smoke emissions from agricultural fires in Mexico and Central
- 522 America. *Journal of Applied Remote Sensing* **2019**, *13*, 1.
- 523 (64) Barnard, J. C.; Volkamer, R.; Kassianov, E. I. Estimation of the mass absorption cross
- 524 section of the organic carbon component of aerosols in the Mexico City Metropolitan
- 525 Area. *Atmospheric Chemistry and Physics* **2008**, *8*, 6665–6679.

526 Graphical TOC Entry



527

Some journals require a graphical entry for the Table of Contents. This should be laid out "print ready" so that the sizing of the text is correct.

Inside the `tocentry` environment, the font used is Helvetica 8 pt, as required by *Journal of the American Chemical Society*.

The surrounding frame is 9 cm by 3.5 cm, which is the maximum permitted for *Journal of the American Chemical Society* graphical table of content entries. The box will not resize if the content is too big: instead it will overflow the edge of the box.

This box and the associated title will always be printed on a separate page at the end of the document.